Aug 24th, 12:00 AM - Aug 25th, 12:00 AM

Active Shear Planes in Block Shear Failure of Bolted Connections

Drew D. A. Clements

Lip H. Teh

Twenty-First International Specialty Conference on Cold-Formed Steel Structures
St. Louis, Missouri, USA, October 24 & 25, 2012

Active Shear Planes in Block Shear Failure of Bolted Connections

Drew D. A. Clements[1] and Lip H. Teh[2]

Abstract

In the AISI Specification for the Design of Cold-formed Steel Structural Members 2007, there are two types of shear planes used to determine the resistance of a bolted connection to block shear failure. When the block shear failure occurs by shear yielding and tensile rupture, the shear failure plane is taken to be the gross shear plane. Conversely, when the block shear failure is deemed to occur by simultaneous shear and tensile ruptures, the shear failure plane is assumed to be the net shear plane. Such an approach is not logical since the shear failure planes should be unique irrespective of the block shear failure mechanism. Through finite element analysis presented in this paper, the shear failure plane is shown to be neither the gross nor the net shear plane, and to be midway between the two shear planes assumed in design specifications. This shear failure plane is termed the active shear plane. The veracity of the active shear area is demonstrated in terms of the ability of the resulting block shear equation to predict the governing failure modes of test specimens consistently, in comparison against the equations assuming the gross and the net shear areas.

Introduction

As described by Teh & Clements (2012), two types of shear planes are used in steel design codes worldwide including the North American Specification for the Design of Cold-formed Steel Structural Members 2007 (AISI 2010) to determine the resistance of a bolted connection to block shear failure. In the

[1]Graduate Structural Engineer, Hatch, 25 Atchinson Street, Wollongong, NSW 2500, AUSTRALIA. Formerly Honours Student, School of Civil, Mining & Environmental Engineering, University Of Wollongong, Wollongong, NSW 2500, AUSTRALIA.
[2]Senior Lecturer, School of Civil, Mining & Environmental Engineering, University Of Wollongong, Wollongong, NSW 2500, AUSTRALIA.

current specification, when the block shear failure occurs by shear yielding and tensile rupture, the shear failure plane is taken to be the gross shear plane. Conversely, when the block shear failure is deemed to occur by simultaneous shear and tensile ruptures, the shear failure plane is assumed to be the net shear plane. The inconsistent definitions of the shear failure planes give rise to unnecessary anomalies that led to repeated amendments to the design provision against block shear failures in the AISC specifications (AISC 1978, 1986, 1999, 2010), from which the AISI provision has been adopted.

In reality, the shear failure planes should be unique as they relate to the same failure mode, irrespective of the block shear failure mechanism. Furthermore, Teh & Clements (2012) have explained that a conventional block shear failure can only occur by the shear yielding and tensile rupture mechanism, as borne out by extensive experimental tests (Hardash & Bjorhovde 1985, Seleim & LaBoube 1996, Teh & Clements 2012). They have also noted the experimental evidence of Franchuk et al. (2003) that suggests the actual shear failure planes to lie midway between the gross and the net shear planes, and proposed a design equation for determining the block shear capacity using the so-called active shear planes.

This paper examines the experimental evidence of Franchuk et al. (2003) through geometrically and materially nonlinear contact finite element analysis using ABAQUS 6.9 (ABAQUS 2009). The active shear planes will also be verified in terms of the ability of the resulting block shear equation to predict the governing failure modes of test specimens consistently, in comparison against the equations assuming the gross and the net shear areas.

Equations for block shear failure strength

The nominal block shear failure strength of a bolted connection is specified in Clause E5.3 of the North American Specification for the Design of Cold-formed Steel Structural Members 2007 (AISI 2010) to be the lesser of the following

$$R_n = 0.6F_y A_{gv} + F_u A_{nt} \tag{1}$$

and

$$R_n = 0.6F_u A_{nv} + F_u A_{nt} \tag{2}$$

in which F_y is the yield stress, A_{gv} is the gross shear area, F_u is the tensile strength, A_{nt} is the net tensile area, and A_{nv} is the net shear area. The regions corresponding to these areas as defined by the code are shown in Figure 1.

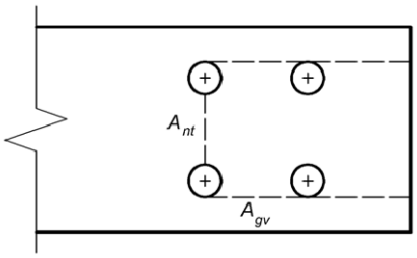

(a) Gross shear planes

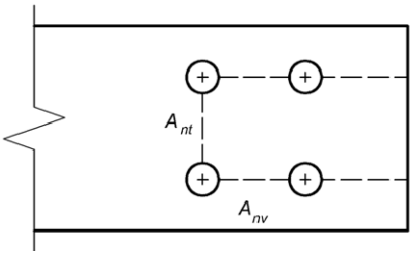

(b) Net shear planes

Figure 1 Gross and net shear planes

Equation (1) represents the block shear failure by shear yielding and tensile rupture, while Equation (2) postulates the simultaneous shear and tensile rupture mechanism. Since Teh & Clements (2012) have ruled out the latter possibility, Equation (2) will be ignored for the rest of this paper.

Eurocode 3 Part 1.8 (ECS 2005) only provides for the shear yielding and tensile rupture mechanism, as reflected in the design equation

$$R_n = {F_y A_{nv}}/{\sqrt{3}} + F_u A_{nt} = 0.577 F_y A_{nv} + F_u A_{nt} \tag{3}$$

which departs from the AISC's long tradition for the shear yielding planes and from the earlier Eurocode (ECS 1992), where the gross shear area was used.

Teh & Clements (2012) have proposed the following equation based on the active shear planes defined in Figure 2

$$R_n = F_u \sum A_{nt}\left(0.9 + 0.1\, d/p_2\right) + 0.6 F_y A_{av} \tag{4}$$

in which variable d denotes the bolt diameter while p_2 is defined in Figure 3.

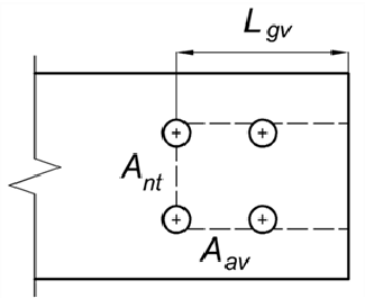

$$L_{av} = L_{gv} - \left(\frac{n_r - 1}{2} + \frac{1}{4}\right) d_h$$

$$\approx L_{gv} - n_r d_h / 2$$

$$A_{av} = 2 L_{av} t$$

Figure 2 Active shear planes

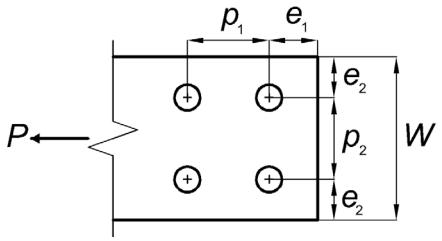

Figure 3 Definitions of geometric variables

Equation (4) incorporates an in-plane "shear lag factor" proposed by Teh & Gilbert (2012) in determining the net section tension capacity. The shear lag factor accounts for the fact that the tensile stresses are not uniformly distributed across the net section, which has a significant effect on the tension capacity of bolted connections in cold-reduced sheet steel.

Finite element analysis to locate the shear failure planes

The finite element models simulate the inner sheet of double-lap bolted connections between steel sheets, an example of which is shown in Figure 4.

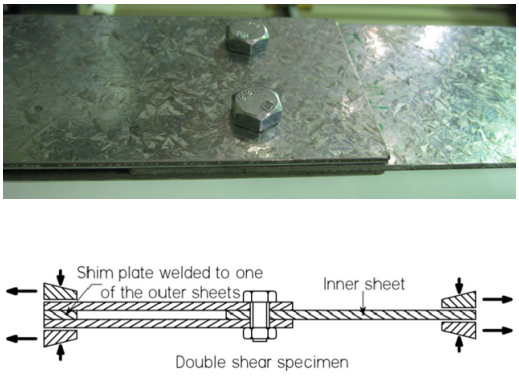

Figure 4 Concentrically loaded inner sheet

Due to symmetry, only half of the concentrically loaded sheet was modelled as shown in Figure 5 with transverse displacements prevented across the symmetry plane. Rotation about the symmetry axis was also prevented. The left end was completely restrained (fixed) and only the mid-plane of the sheet, indicated by the lines running along the middle of the sheet thickness, was restrained out-of-plane so that necking through the sheet thickness was not prevented.

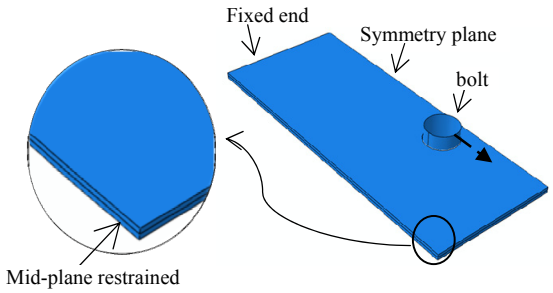

Figure 5 Conceptual model (one row of bolts)

The hexahedral reduced integration brick element type C3D8R available in ABAQUS 6.9 (ABAQUS 2009) was used. An example of the finite element mesh is shown in Figure 6.

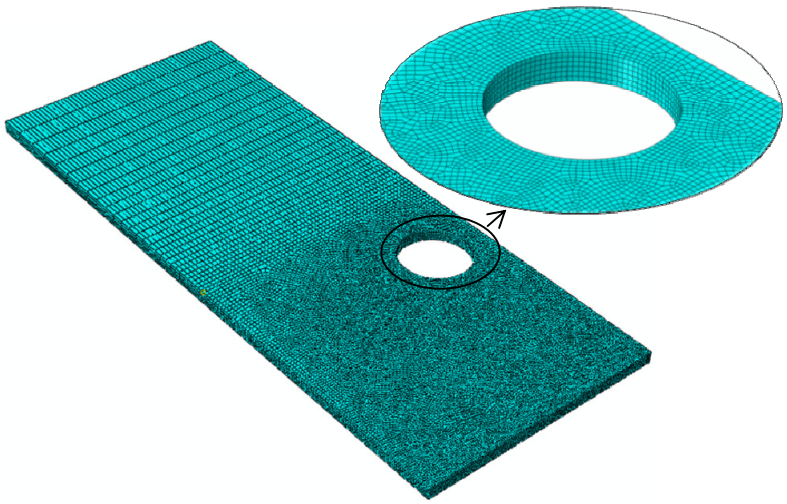

Figure 6 Finite brick element (C3D8R) mesh

The analysis was geometrically and materially nonlinear using the true stress-strain curves shown in Figure 7. The plasticity of the steel material was handled through the von Mises yield criterion and the Prandtl-Reuss flow rule with isotropic hardening. The true shear yield stress τ_y of the 1.5-mm sheet steel is therefore approximately 355 MPa, and that of the 3.0-mm sheet steel is 320 MPa. The Poisson's ratio is assumed to be 0.3.

Loading of the connection was simulated by displacing the bolt away from the fixed end as indicated by the dashed arrow in Figure 5, which would be resisted by the contact surface between the bolt and the bolt hole at the downstream end. The bolt was modelled as a 3D analytical rigid body revolved shell, and the bolt hole had a diameter that was 1 mm larger than the bolt, as was the case with the laboratory test specimens.

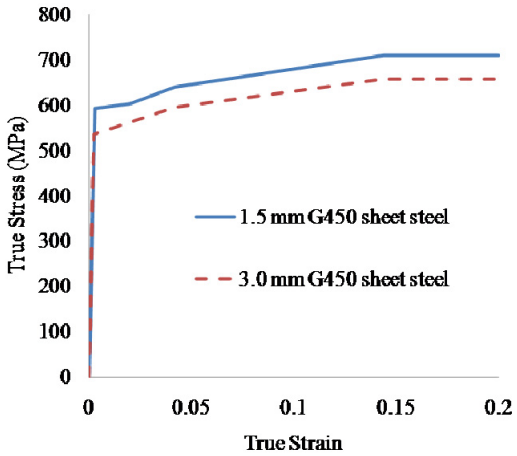

Figure 7 Modelling of material behaviour

Figure 8 shows the two basic bolting configurations studied in the present work, which were tested by Teh & Clements (2012). The measured material properties of the specimens are given in Table 1, while their nominal geometric dimensions as defined in Figure 3 are given in Tables 2 and 3, which also list the professional factors of the finite element analysis results. The variable P_t in the tables denotes the ultimate test loads obtained in the experiment of Teh & Clements (2012). It can be seen that the finite element models were able to estimate the block shear failure loads with reasonable accuracy.

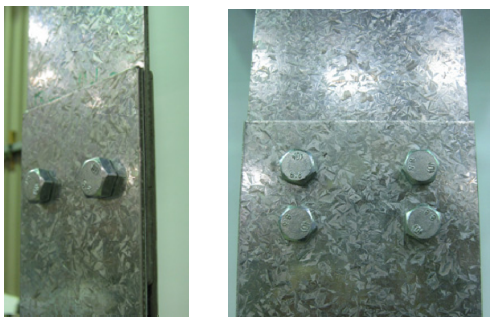

(a) Series A (b) Series B

Figure 8 Bolting configurations of Series A and B specimens

Table 1 Measured engineering properties

	t_{base} (mm)	F_y (MPa)	F_u (MPa)	F_u / F_y	ε_{15} (%)	ε_{25} (%)	ε_{50} (%)	ε_{uo} (%)
1.5 mm	1.48	605	630	1.04	21.3	18.0	12.0	6.8
3.0 mm	2.95	530	580	1.09	29.3	22.0	15.3	8.1

Table 2 Professional factors for Series A specimens (with 17 mm bolt holes)

Spec	W (mm)	p_2 (mm)	t (mm)	e_1 (mm)	P_t/FEA
CPD14	100	33	1.5	50	1.10
CPD16	100	33	3.0	50	1.05
CPD18	120	40	1.5	50	0.99
CPD20a	120	40	3.0	50	0.98
CPD20b	120	40	3.0	50	0.98
CPD22a	100	26	1.5	50	1.14
CPD22b	100	26	1.5	50	1.11
CPD24a	100	26	3.0	50	1.05
CPD24b	100	26	3.0	50	1.04
CPD26a	120	26	1.5	50	1.06
CPD26b	120	26	1.5	50	1.07
CPD28a	120	26	3.0	50	1.03
CPD28b	120	26	3.0	50	1.05
CPD36	130	45	3.0	30	1.03
				Mean	1.05
				COV	0.044

Table 3 Professional factors for Series B specimens (p_1 = 30 mm)

Spec	W (mm)	p_2 (mm)	t (mm)	e_1 (mm)	d_h (mm)	P_t/FEA
CQ2a	120	26	1.5	50	17	1.09
CQ2b	120	26	1.5	50	17	1.07
CQ3	120	26	3.0	50	13	1.03
CQ4	120	26	3.0	50	17	1.03
CQ5a	130	40	1.5	30	13	1.02
CQ5b	130	40	1.5	30	13	1.04
CQ6a	130	40	1.5	30	17	1.07
CQ6b	130	40	1.5	30	17	1.06
CQ7	130	40	3.0	30	13	1.00
CQ8	130	40	3.0	30	17	1.04
CQ9b	130	55	1.5	30	13	1.07
CQ10a	130	55	1.5	30	17	1.06
CQ10b	130	55	1.5	30	17	1.05
CQ11	130	55	3.0	30	13	0.99
CQ12	130	55	3.0	30	17	1.04
					Mean	1.04
					COV	0.027

Figure 9(a) shows the longitudinal true normal stress contours of Specimen CPD14. It is evident that the tensile stresses are not uniform across the net section between the two bolt holes (the symmetry plane is on the left-hand side).

Figure 9(b) shows the longitudinal true in-plane shear stress contours corresponding to the normal stress contours in Figure 9(a). It can be seen that the largest shear stresses take place along a shear plane that is midway between the gross and the net shear planes indicated in Figure 1. The active shear planes depicted in Figure 2 represent the FEA results most closely.

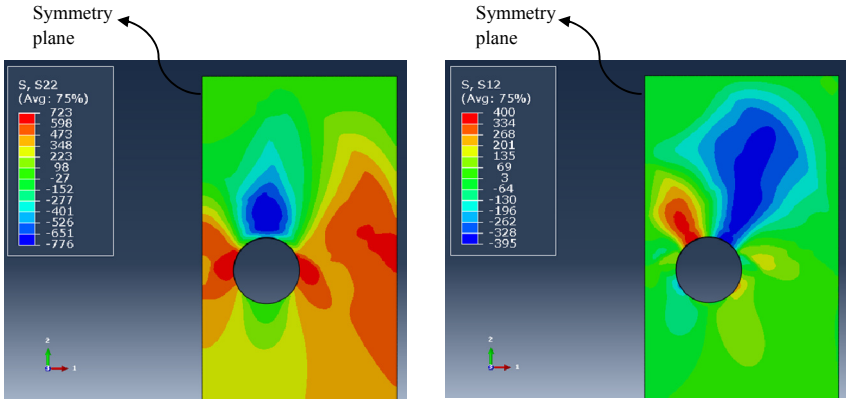

(a) Longitudinal normal stress (b) Longitudinal shear stress

Figure 9 Longitudinal normal stresses and in-plane shear stresses of CPD14

It can also be seen from Figure 9(b) that the largest shear stresses only take place within a short portion of each active shear plane, with the shear stresses approaching zero towards the downstream end. As shown in Figure 2, the active shear area A_{av} in Equation (3) is calculated by ignoring a portion of each active shear plane over a length equal to a quarter of the bolt hole diameter. This neglect is supported by the shear stress contours in Figure 9(b).

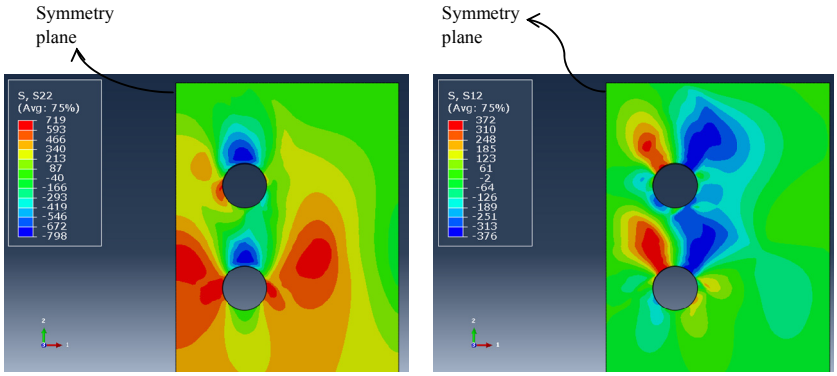

(a) Longitudinal normal stress (b) Longitudinal shear stress

Figure 10 Longitudinal normal stresses and in-plane shear stresses of CQ5

Figures 10(a) and 10(b) show the longitudinal true normal stress and the true in-plane shear stress contours of Specimen CQ5. It can be seen that the active shear planes are still best represented by Figure 2. The shear stress contours also support the formula for determining the active shear area A_{av} shown in Figure 2.

Further verification of the active shear planes

Teh & Clements (2012) have shown that Equation (4), which makes use of the active shear planes defined in Figure 2, is significantly more accurate than Equations (1) and (3) in estimating the block shear failure loads. Hypothetically, an incorrect equation may give more accurate estimates than a correct equation does if the material and/or geometric properties used in the calculations are not accurate representations of the actual specimens. In fact, if the nominal material properties of the G450 sheet steels are used in the calculations, then Equation (1) would be found to give more accurate results than Equation (4). In theory, it is possible, for example, that the measured tensile strengths used in the calculations were too high, skewing the results in favour of Equation (4) against Equation (1).

The veracity of the active shear planes defined in Figure 2 is demonstrated by checking the ability of Equation (4) to predict the governing failure modes of test specimens consistently, in comparison against Equations (1) and (3). The governing failure mode is identified by comparing the block shear capacity against the net section tension capacity, both computed using the same measured material and geometric properties.

Each of the competing block shear capacity equations is compared against the net section tension capacity given by

$$R_n = F_u \left[\sum A_{ni} \left(0.9 + 0.1 \, d \big/ p_2 \right) + \sum A_{no} \left(0.9 + 0.05 \, d \big/ e_2 \right) \right] \qquad (5)$$

in which A_{ni} refers to a net section between bolt holes, and A_{no} refers to either of the two net sections flanking the group of bolts. The variables p_2 and e_2 are defined in Figure 3. Equation (5) has been demonstrated by Teh & Gilbert (2012) to predict the net section tension capacity of bolted connections in the present steel materials with very high accuracy.

All the specimens in Tables 4 and 5 failed in block shear. A cross sign "×" in a cell of these tables indicates that the equation wrongly predicts the governing failure mode to be net section fracture. Equation (1) missed the block shear

failure mode of most specimens as it overestimates the shear yielding resistance to block shear failure due to its use of the gross shear planes depicted in Figure 1(a), especially for the specimens with multiple rows of bolts.

Table 4 Predicted failure modes for Series A specimens failing in block shear

Spec	W (mm)	p_2 (mm)	t (mm)	e_1 (mm)	d_h (mm)	With Equation (5)		
						(1)	(3)	(4)
CPD14	100	33	1.5	50	17	×	√	√
CPD15	100	33	3.0	50	13	×	√	√
CPD16	100	33	3.0	50	17	×	√	√
CPD18	120	40	1.5	50	17	×	√	√
CPD19	120	40	3.0	50	13	√	√	√
CPD20a	120	40	3.0	50	17	√	√	√
CPD20b	120	40	3.0	50	17	√	√	√
CPD22a	100	26	1.5	50	17	×	√	√
CPD22b	100	26	1.5	50	17	×	√	√
CPD23a	100	26	3.0	50	13	×	√	√
CPD23b	100	26	3.0	50	13	×	√	√
CPD24a	100	26	3.0	50	17	×	√	√
CPD24b	100	26	3.0	50	17	×	√	√
CPD26a	120	26	1.5	50	17	√	√	√
CPD26b	120	26	1.5	50	17	√	√	√
CPD27	120	26	3.0	50	13	√	√	√
CPD28a	120	26	3.0	50	17	√	√	√
CPD28b	120	26	3.0	50	17	√	√	√
CPD36	130	45	3.0	30	17	√	√	√
					Misses	10	0	0

Table 5 Predicted failure modes for Series B specimens failing in block shear

Spec	W (mm)	p_2 (mm)	t (mm)	e_1 (mm)	d_h (mm)	With Equation (5)		
						(1)	(3)	(4)
CQ2a	120	26	1.5	50	17	×	√	*
CQ2b	120	26	1.5	50	17	×	√	*
CQ3	120	26	3.0	50	13	×	√	√
CQ4	120	26	3.0	50	17	×	√	√
CQ5a	130	40	1.5	30	13	×	√	√
CQ5b	130	40	1.5	30	13	×	√	√
CQ6a	130	40	1.5	30	17	×	√	√
CQ6b	130	40	1.5	30	17	×	√	√
CQ7	130	40	3.0	30	13	√	√	√
CQ8	130	40	3.0	30	17	×	√	√
CQ9b	130	55	1.5	30	13	×	√	√
CQ10a	130	55	1.5	30	17	×	√	√
CQ10b	130	55	1.5	30	17	×	√	√
CQ11	130	55	3.0	30	13	×	√	√
CQ12	130	55	3.0	30	17	×	√	√
CQ17	120	45	1.5	30	13	×	√	√
CQ18	130	50	1.5	30	13	×	√	√
CQ19	120	55	3.0	25	13	×	√	√
CQ20	120	55	3.0	25	17	×	√	√
					Misses	18	0	0

If the shear lag factor is applied to the tensile resistance term of Equation (1), the total number of misses would decrease by six to 22. If the shear lag factor in Equation (4) is neglected, reducing the equation into the conventional net section tension capacity where the net section is assumed to be fully effective, the number of misses would decrease by ten to 18.

All the four specimens in Table 6 failed in net section fracture. A cross sign "×" in a cell indicates that the equation wrongly predicts the specimen to fail in block shear. Equation (3) missed the net section tension fracture mode of all specimens as it underestimates the shear yielding resistance to block shear failure due to its use of the net shear planes depicted in Figure 1(b).

Table 6 Predicted failure modes for specimens failing in net section fracture

Spec	W (mm)	p_2 (mm)	t (mm)	e_1 (mm)	d_h (mm)	With Equation (5)		
						(1)	(3)	(4)
CQ1a	120	26	1.5	50	13	√	×	√
CQ1b	120	26	1.5	50	13	√	×	√
CQ14	130	65	1.5	30	17	√	×	√
CQ16	130	65	3.0	30	17	√	×	√
					Misses	0	4	0

The only equation that never predicted an incorrect failure mode is Equation (4). For Specimens CQ2a and CQ2b in Table 5, the block shear capacity given by the equation is the same as the net section tension capacity given by Equation (5).

Conclusions

This paper uses geometrically and materially nonlinear contact finite element analysis to confirm that the active shear planes in block shear failure of bolted connections lie between the gross and the net shear planes, as indicated by the experimental evidence obtained by other researchers. The finite element analysis results also indicate that the in-plane shear stresses approach zero towards the downstream end of the connection.

The use of the active shear planes is shown to correctly predict the governing failure modes of all test specimens, whether block shear failure or net section fracture, in contrast to the use of the gross or the net shear planes. The present work resolves the hypothetical uncertainty whether the measured material (and geometric) properties used in the calculations of the block shear capacities, which were significantly different from the nominal values, unduly favour the equation proposed by the authors in comparing the professional factors.

The block shear equation previously proposed by the authors, which makes use of the active shear planes, is supported by the present finite element analysis results and the present comparison against alternative equations in predicting the correct failure modes, in addition to independent experimental evidence and the authors' previous demonstration of the equation's accuracy in estimating the block shear failure loads of laboratory test specimens.

References

ABAQUS (2009) ABAQUS Analysis User's Manual, Version 6.9, Dassault Systèmes, Providence RI.

AISC (1978) *Specification for the Design, Fabrication and Erection of Structural Steel for Buildings*, American Institute of Steel Construction, Chicago IL.

AISC (1986) *Load and Resistance Factor Design Specification for Structural Steel Buildings*, American Institute of Steel Construction, Chicago IL.

AISC (1999) *Load and Resistance Factor Design Specification for Structural Steel Buildings*, American Institute of Steel Construction, Chicago IL.

AISC (2010) *Specification for Structural Steel Buildings*, ANSI/AISC 360-10, American Institute of Steel Construction, Chicago IL.

AISI (2010) *Supplement No. 2 to the North American Specification for the Design of Cold-formed Steel Structural Members 2007 Edition*, American Iron and Steel Institute, Washington DC.

ECS (1992) *Eurocode 3: Design of steel structures, Part 1.8: Design of joints*, EN 1993-1-8, European Committee for Standardisation, Brussels, Belgium.

ECS (2005) *Eurocode 3: Design of steel structures, Part 1.8: Design of joints*, EN 1993-1-8, European Committee for Standardisation, Brussels, Belgium.

Franchuk, C. R., Driver, R. G., and Grondin, G. Y. (2003) "Experimental investigation of block shear failure in coped steel beams." *Can. J. Civ. Eng.*, 30, 871-881.

Hardash, S. G., and Bjorhovde, R. (1985) "New design criteria for gusset plates in tension." *Engineering Journal AISC*, 22 (2), 77-94.

Seleim, S., and LaBoube, R.A. (1996) "Behavior of low ductility steels in cold-formed steel connections." *Thin-Walled Structures*, 25 (2), 135-150.

Teh, L. H., and Clements, D. D. A. (2012) "Block shear capacity of bolted connections in cold-reduced steel sheets," scheduled for publication in April 2012 in *J. Struct. Eng*., ASCE.

Teh, L. H., and Gilbert, B. P. (2012) "Net section tension capacity of bolted connections in cold-reduced steel sheets," *J. Struct. Eng.*, 138 (3), 337-344.